Online Voltage Sensorless High-Resistance Connection Diagnosis in Induction Motor Drives

Pablo M. de la Barrera, *Member, IEEE*, Guillermo R. Bossio, *Member, IEEE*, and Roberto Leidhold, *Member, IEEE*

***Abstract*—A new method for online high-resistance connection (HRC) diagnosis in induction motor (IM) drives is presented in this effort. This voltage sensorless method is based on a signal injection strategy applied to the IM during its normal operation. The signal is injected in the d-axis in such a way that it provides the phase currents with a dc component while avoiding torque perturbation. By measuring phase currents, it is possible to detect and isolate HRC problems. Experimental results showing high sensitivity to HRCs and immunity to symmetrical stator resistance variations have been obtained in a laboratory setup. The low perturbation produced by the injection method over the IM variables has also been experimentally demonstrated.**

***Index Terms*—Fault diagnosis, high-resistance connection (HRC), induction motor (IM) drive, signal injection.**

Nomenclature

*	Reference value.
$^-$	Mean value.
$i_{\mathrm{dinj}}, i_{\mathrm{qinj}}$	Injected current in dq reference frame.
$i_{\alpha\mathrm{dc}}, i_{\beta\mathrm{dc}}$	DC in $\alpha\beta$ reference frame.
$i_{\alpha\mathrm{inj}}, i_{\beta\mathrm{inj}}$	Injected current in $\alpha\beta$ reference frame.
i_A, i_B, i_C	Phase currents.
u_A, u_B, u_C	Phase voltages.
U_{dc}	DC link voltage.
Δ	Difference between ideal and actual signals.
t_d	Dead time.
T_s	Switching period.
$\mathbf{i}_{ABC\mathrm{DC}}$	DC component of phase currents (vector).
$\mathbf{u}_{ABC\mathrm{DC}}$	DC component of phase voltages (vector).
R_A, R_B, R_C	Phase resistances.
$\mathbf{R}_{\mathrm{HRC}}$	HRC indicator.
$\mathbf{P}$	Transformation for projecting three phase quantities into $\mathbf{R}_{\mathrm{HRC}}$ plane.
R_s	Symmetric stator resistance.
ΔR	Connection resistance.
$\mathrm{v}_1, \mathrm{v}_2, \mathrm{v}_3, \mathrm{v}_4, \mathrm{v}_5, \mathrm{v}_6$	Possible vectors for the injection.
e	Percentage relative error.
$\sigma_{\mathbf{R}_{\mathrm{HRC}}}$	Angle of the indicator vector.
λ	Limit value for the HRC alarm.

Manuscript received May 9, 2014; revised September 1, 2014 and October 28, 2014; accepted November 12, 2014. Date of publication December 22, 2014; date of current version May 15, 2015. This work was supported in part by the Universidad Nacional de Río Cuarto, in part by the Fondo para la Investigación Científica y Tecnológica-Agencia Nacional de Promoción Científica y Tecnológica, in part by the Consejo Nacional de Investigaciones Científicas y Técnicas, and in part by the German Research Foundation.

P. M. de la Barrera and G. R. Bossio are with the Grupo de Electrónica Aplicada, Facultad de Ingeniería, Universidad Nacional de Río Cuarto, Río Cuarto X5804BYA, Argentina, and also with the CONICET, Buenos Aires C1033AAJ, Argentina (e-mail: pbarrera@ieee.org; gbossio@ing.unrc.edu.ar).

R. Leidhold is with the Institute for Electric Power Systems, Otto-von-Guericke-Universitaet Magdeburg, 39106 Magdeburg, Germany (e-mail: roberto.leidhold@ovgu.de).

Color versions of one or more of the figures in this paper are available online at http://ieeexplore.ieee.org.

Digital Object Identifier 10.1109/TIE.2014.2385038

I. Introduction

CONDITION monitoring and fault diagnosis of induction motor (IM) have become one of the most important topics in industry throughout the last decades [1]. This concern is due to the high economic losses produced by unscheduled process downtime as a consequence of faults in IM. These losses usually outweigh the cost of the motor maintenance. Therefore, several fault detection and diagnosis methods based on currents, torque, power, vibration, or external magnetic flux, among other physical quantities, have been developed [2]–[6].

The use of electric drives increases the stress on the machine and its power circuits, reducing the life span of the machine. Electrical, mechanical, and thermal stresses appear on the windings, bearings, and stator core of the machine, increasing the possibilities of failure [7]. However, electric drives allow the development of new fault-tolerant control strategies to improve the reliability [8]–[10].

All the conductors and connections between the power source and the IM are called power circuits. The most important problems in this part of the circuit appear in the connections (as it was expressed in [11] approximately 80% of the power circuit problems).

High-resistance connection (HRC) is a progressive fault in which some factors (e.g., high current or voltage, vibration, chemicals, or dirt in the atmosphere, metal fatigue, aging, or extreme ambient temperature) initiate a degradation mechanism. As it was shown in [12], this mechanism can be schematized by two main positive feedback loops in which the contact resistance increment produces contact temperature rise. This temperature rise generates thermal expansion and the acceleration of the oxidation and/or corrosion. Both aforementioned effects cause an increase in contact resistance; thereby, the positive feedback for the degradation of a power connection is generated.

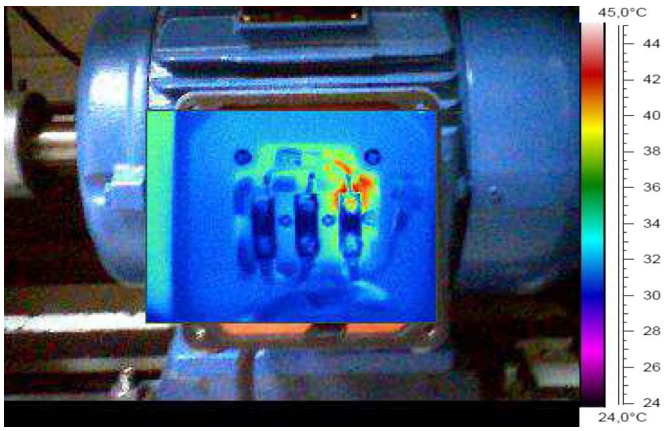

Fig. 1. IR thermography of an IM with HRC in one of its terminals [13].

If the feedback is not stopped, it can result in uncontrollable overheating. For instance, Fig. 1 shows an infrared thermography of an IM with an overheating terminal [13]. This would be the precursor of arc flash, connection and cable melting, and even an electrical fire, causing not only equipment and building losses but also personal injuries [14].

The increment in the contact resistance also produces an unbalanced supply voltage of the IM. Different effects will be present depending on the IM drives used (open or closed loop). In the case of open-loop drives, an asymmetry in the IM phases (stator turn fault or increase in contact resistance) produces similar effects as those in an IM fed by the grid. Namely, negative sequence currents flow in the IM that, in addition, produce an oscillating torque at twice the fundamental frequency while reducing the IM efficiency.

As far as closed-loop drives are concerned, the effects produced by a stator asymmetry over the IM are quite different compared with those of the open-loop drives. Closed-loop drives cover the typical characteristics produced by a stator asymmetry (negative sequence current and oscillating torque) due to its current and speed regulators, thereby increasing the complexity of the analysis and interpretations of the results [15].

Therefore, to detect and diagnose HRC problems, different methods have been proposed. The most widespread methods for HRC are the voltage drop survey and the infrared thermography [16], [17]. The first one is a simple, quick, and cheap method based on comparing the magnitude of the voltage drop in each phase in the loaded IM to detect HRC. When the IM is fed by the grid, only a true RMS voltmeter is required for performing the method. Nevertheless, in the case of inverter fed machines, special voltmeters are required because standard multimeters usually give erroneous results due to the pulsewidth modulation (PWM) [13].

IR thermography is a quick and reliable method for detecting hot spots in different IM drive components. A disadvantage of this method is the cost of the infrared camera and those associated to the plant inspection and the postprocessing of the images.

Both mentioned methods must be performed by a specialist, being the automation of the detection and diagnosis process very difficult.

To improve the diagnosis process, HRC diagnosis methods suitable for IM drives have been reported in literature throughout the last two years. Proposed methods can be classified in offline and online ones. On one hand, offline methods require taking the drives out of service for the diagnosis. Some offline methods of HRC diagnosis are based on signal injection [12], [18]–[20]. On the other hand, online methods perform the diagnosis, whereas the IM drives are operating. The proposed methods were based on wavelet [21], [22], multireference frame controllers [23], [24], and negative sequence regulators [25], [26].

In [13], an online HRC diagnosis method for IM drives that use signal injection has been proposed. As in [12], the voltage of the motor neutral point is used for the detection. For this reason, these methods require access to the neutral point, and they are applicable only to motors with star connection.

Therefore, a new online voltage sensorless HRC diagnosis method for IM drives based on dc signal injection is proposed in the present effort. This method does not require the voltage measurement as in [12] and [13]. For this reason, the number of sensors is reduced, making it possible to implement the diagnosis method in motors with both star and delta connections. In certain time lengths, a predefined dc exploratory signal is injected to the power circuits of the IM drive during its normal operation.

Although, the dc signal injection has been previously used, e.g., for estimating the stator temperature, by means of the stator resistance [27], this proposal produces torque oscillation as a side effect. The present proposal for HRC diagnosis solves the aforementioned problem of torque oscillation.

The effect produced by this injected signal over the IM power circuits is analyzed by using a fault indicator, which is calculated with reference voltage and current information.

The proposal was experimentally validated in a laboratory prototype, demonstrating high sensitivity to the HRC in one and two phases of the IM. The immunity of the indicator to symmetric variations of IM stator resistance, as well as stator winding turn fault (which produces inductance variations), has also been shown. In addition, the effects produced by the improved dc signal injection were analyzed, showing small perturbations over the IM speed and currents. Finally, based on the fault indicator, a fault detection and isolation (FDI) algorithm is proposed, and the methodology to determine limits for the HRC alarms is presented.

This paper is organized as follows. Section II presents the method for HRC diagnosis using signal injection and its effects over the normal operation of the IM drive. The experimental setup and the obtained results are presented in Section III. Section IV presents an FDI algorithm proposed for diagnosing HRC problems. Finally, some conclusions and final remarks are drawn in Section V.

II. High-Resistance Connection Diagnosis Method

A method to detect HRC online is presented here. A detailed description of the injected signal and the proposed HRC indicator is shown. Furthermore, the analysis of the effect

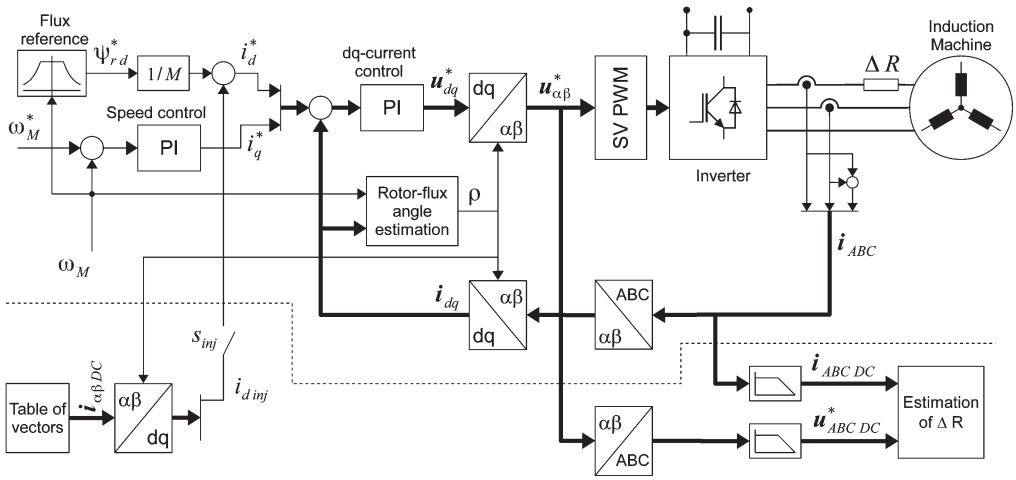

Fig. 2. Block diagram of the online HRC diagnosis method.

of inverter nonlinearities on the diagnosis is presented in the following.

A. Signal Injection

The proposed method makes it possible to determine HRC problems in IM drives based on the injection of predefined current vectors imposed by the three-phase inverter. This method is applied during the normal operation of the IM (online method).

A block diagram of the proposed method is presented in Fig. 2. In the upper part of the figure, the block diagram of a conventional field-oriented control for IM is shown. The connection of the IM with the inverter includes a cable and connection devices such as terminal boxes and connectors, which are subject to HRC failures. The HRC failure is represented in the diagram with the resistance ΔR.

The inverter is driven by a conventional space-vector PWM. The voltage reference feeding the PWM is generated by a current controller, implemented in the rotor-flux oriented reference frame. The angle of the rotor flux is estimated based on the measured currents and the rotor angle or speed.

The q-component of the reference current is generated by a speed controller, whereas the d-component is driven by a flux reference block. The flux reference is kept constant at its rated value for speeds under the rated one and with a field-weakening rule for speeds beyond the rated one, as usual. Since the flux reference is slowly changing, a flux control loop is not required. Consequently, the d-component of the current reference is directly generated by $i_d^\star = \psi_{rd}^\star / M$.

To estimate the asymmetry of the resistance without being perturbed by asymmetries of the inductance, the injection of a dc in the stationary $(\alpha\beta)$ reference frame is the best option. As the current control is implemented in the rotor-flux (dq) reference frame, the dc signals have to be transformed before being added to the current reference (hereafter called direct dc signal injection), i.e.,

$$i_{\mathrm{dinj}} = i_{\alpha\mathrm{dc}} \cos(\theta) + i_{\beta\mathrm{dc}} \sin(\theta) \tag{1}$$

$$i_{\mathrm{qinj}} = -i_{\alpha\mathrm{dc}} \sin(\theta) + i_{\beta\mathrm{dc}} \cos(\theta). \tag{2}$$

The dc injected in the $\alpha\beta$ reference frame are oscillating in the dq reference frame with fundamental frequency. This means that the flux producing current (i_d) generates an oscillating component in the rotor flux. However, this oscillating component is filtered by the rotor time constant. Consequently, at speeds above approximately 50% of the rated one, the oscillating component of i_d will have negligible effects on the flux.

The oscillating component of the torque producing current i_q would result in a torque ripple and, consequently, in a speed ripple. To avoid this, the injected q-component is set to zero, and only the d-component is injected (hereafter called improved dc signal injection), i.e.,

$$i_{\mathrm{dinj}} = i_{\alpha\mathrm{dc}} \cos(\theta) + i_{\beta\mathrm{dc}} \sin(\theta) \tag{3}$$

$$i_{\mathrm{qinj}} = 0. \tag{4}$$

By transforming i_{dinj} and i_{qinj} as defined in (3) and (4) back to the $\alpha\beta$ reference frame, as

$$\begin{bmatrix} i_{\alpha\mathrm{inj}} \\ i_{\beta\mathrm{inj}} \end{bmatrix} = \begin{bmatrix} \cos(\theta) & -\sin(\theta) \\ \sin(\theta) & \cos(\theta) \end{bmatrix} \begin{bmatrix} i_{\mathrm{dinj}} \\ i_{\mathrm{qinj}} \end{bmatrix} \tag{5}$$

and by applying trigonometric equivalences, the resulting injected signal yields

$$i_{\alpha\mathrm{inj}} = \frac{1}{2} i_{\alpha\mathrm{dc}} + \frac{1}{2} i_{\alpha\mathrm{dc}} \cos(2\theta) + \frac{1}{2} i_{\beta\mathrm{dc}} \sin(2\theta) \tag{6}$$

$$i_{\beta\mathrm{inj}} = \frac{1}{2} i_{\beta\mathrm{dc}} + \frac{1}{2} i_{\alpha\mathrm{dc}} \sin(2\theta) - \frac{1}{2} i_{\beta\mathrm{dc}} \cos(2\theta). \tag{7}$$

The actual added signals in $\alpha\beta$ have a dc component of half of the amplitude and contain an oscillating component; however, they will not produce torque ripple. Only the dc component is relevant for estimating the resistance asymmetry. The above described strategy is shown in the bottom left of Fig. 2. There, a table with the signal vectors that are applied in turns for resistance estimation is implemented. The dc signals are then transformed to the dq-reference frame, but only the d-component is added to the current reference as to avoid torque ripple.

To avoid ripple in the rotor flux, the signal i_{dinj} is injected only when the speed is over a certain threshold (using s_{inj} in Fig. 2).

The response to the injected signal is evaluated from the measured phase currents and voltage references, as it can be seen in the bottom right of Fig. 2. The voltage reference in the $\alpha\beta$-reference frame is transformed to phase values and low-pass filtered. Similarly, the measured phase currents are low-pass filtered. The cutoff frequency of the filters is set much lower than the minimal fundamental frequency (pole pairs times speed threshold for s_{inj}) to obtain the dc component. To reduce the computational effort, the filters are implemented in two stages. The signals are initially filtered with a second-order filter, then downsampled and filtered again with a second-order filter in the lower sampling rate.

B. Effect of Inverter Nonlinearities

The voltage used for computing the resistance asymmetry is taken from the reference value of the PWM. Due to the inverter nonlinearities, the actual voltage (switching-cycle average) will differ from the reference, particularly at a low modulation index [28]. The voltage difference is mainly due to the dead time and the voltage drop of the semiconductors. Considering an insulated-gate bipolar transistor (IGBT)-based inverter, the latter are the collector–emitter saturation voltage $U_{\text{CE(sat)}}$ for the IGBT and the forward voltage U_f for the free-willing diode. Assuming $U_f = U_{\text{CE(sat)}}$, the voltage difference for phase A yields [29]

$$\Delta u_A = u_A - u_A^* = U_d \operatorname{sgn}(i_A) \tag{8}$$

with the constant amplitude

$$U_d = \frac{t_d}{T_s} U_{\text{dc}} + U_{\text{CE(sat)}} \tag{9}$$

where u_A^* and u_A are the reference and actual voltages of phase A, respectively; i_A is the current of phase A; t_d is the dead time; T_s is the switching period; and U_{dc} is the dc-link voltage.

The case of a sinusoidal current without offset is considered in Fig. 3. The current and its mean value are shown in Fig. 3(a). The reference and actual (switching-cycle average) voltages are shown in Fig. 3(b). The resulting voltage difference Δu_A shown in Fig. 3(c) is a square wave with the same duration of the positive and negative half-cycles (symmetrical wave), which is determined by the zero crossings of the current. Consequently, the mean voltage difference $\overline{\Delta u_A}$ is zero.

The case of a sinusoidal current with a positive offset due to the injected signal is considered in Fig. 4. The current and its mean value are shown in Fig. 4(a), whereas the reference and actual voltages are shown in Fig. 4(b). As in the previous case, Δu_A is also determined by the zero crossings of the current, but it is not a symmetrical square wave. The width of the positive half-cycle increases by twice the angle α, as shown in Fig. 4(c). By analyzing the figure, the angle α can be deduced as

$$\alpha = \sin^{-1}\left(\frac{i_{\text{ADC}}}{\hat{i}_A}\right) \tag{10}$$

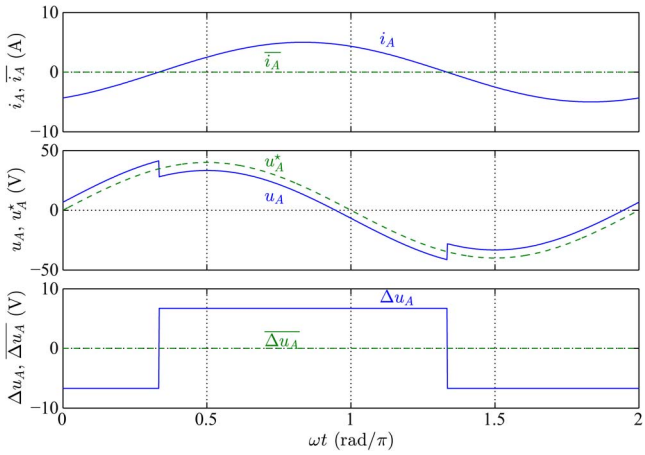

Fig. 3. Analytical results for the effect of inverter nonlinearities without injected dc signal, (a) instantaneous and mean current, (b) voltage reference and actual voltage, and (c) instantaneous voltage drop and mean voltage drop.

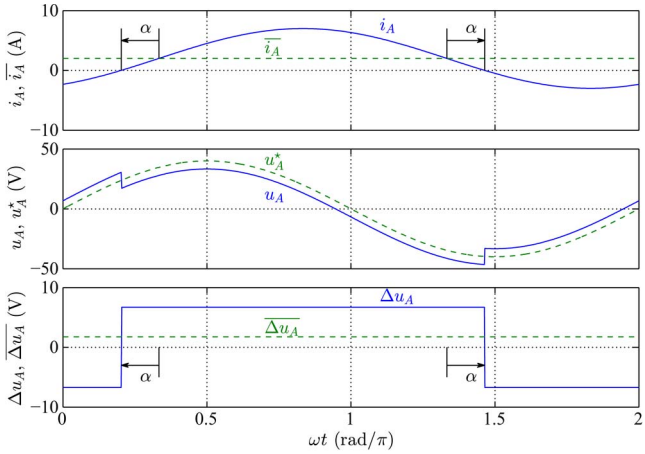

Fig. 4. Analytical results for the effect of inverter nonlinearities with injected dc signal, (a) instantaneous and mean current, (b) voltage reference and actual voltage, and (c) instantaneous voltage drop and mean voltage drop.

where $\hat{i}_A$ is the peak of the ac component of the current. The wider half-cycle results in a higher mean voltage difference $\overline{\Delta u_A}$, yielding

$$\overline{\Delta u_A} = \frac{2U_d}{\pi}\alpha = \frac{2U_d}{\pi}\sin^{-1}\left(\frac{i_{\text{ADC}}}{\hat{i}_A}\right). \tag{11}$$

If the dc-injected signal is small compared with the peak current, then (11) can be approximated by

$$\overline{\Delta u_A} = \frac{2U_d}{\pi}\frac{i_{\text{ADC}}}{\hat{i}_A}. \tag{12}$$

The same result is obtained for the other phases. It can be concluded that for a given ac, the mean voltage difference is proportional to the mean current i_{ADC}. This is a resistive effect for the dc-injected signal, which is the same for all phases. Consequently, it will not affect the estimation of the resistance asymmetry.

TABLE I
POSSIBLE VECTORS FOR THE INJECTION IN ABC AND $\alpha\beta$ VARIABLES

Case	$\mathbf{i}_{ABCDC}$ A			$\mathbf{i}_{\alpha\beta DC}$ A	
	A	B	C	α	β
v_1	1.0	-1.0	0.0	1	$-\frac{1}{\sqrt{3}}$
v_2	-1.0	1.0	0.0	-1	$\frac{1}{\sqrt{3}}$
v_3	1.0	0.0	-1.0	1	$\frac{1}{\sqrt{3}}$
v_4	-1.0	0.0	1.0	-1	$-\frac{1}{\sqrt{3}}$
v_5	0.0	1.0	-1.0	0.0	$\frac{2}{\sqrt{3}}$
v_6	0.0	-1.0	1.0	$\frac{1}{3}$	$-\frac{1}{\sqrt{3}}$

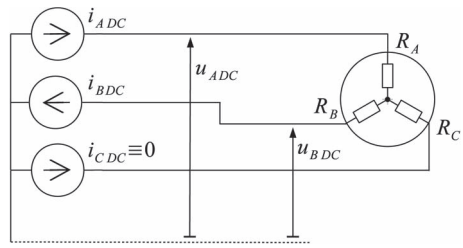

Fig. 5. Simplified equivalent circuit during the injection of vector v_1.

C. HRC Indicator

Based on the aforementioned signal injection strategy, the contact resistance can be estimated by using the information of the dc component of phase currents $\mathbf{i}_{ABCDC}$ and voltages $\mathbf{u}_{ABCDC}$ (see Fig. 2).

Depending on the injected signal case of Table I, equivalent resistance between phases can be calculated. Fig. 5 shows the equivalent circuit of the IM under the dc excitation in steady state for v_1. By inspecting Fig. 5, the following expression can be obtained:

$$u_{ABDC} = i_{ADC}\, R_{AB} \tag{13}$$

where $i_{ADC} = i_{BDC}$ and $i_{CDC} = 0$, the line voltage u_{ABDC} can be calculated based on phase voltages as $u_{ABDC} = (u_{ADC} - u_{BDC})$, and the resistance between phases is $R_{AB} = (R_A + R_B)$.

In this way, for evaluating the per-phase equivalent resistances of the IM, at least three different injected vectors are required to obtain a set of three linear and independent equations. Therefore, for vectors v_3 and v_5, the following expressions are obtained:

$$u_{ACDC} = i_{ADC}\, R_{AC} \tag{14}$$

$$u_{BCDC} = i_{BDC}\, R_{BC} \tag{15}$$

where line voltages can be calculated as $u_{ACDC} = (u_{ADC} - u_{CDC})$ and $u_{BCDC} = (u_{BDC} - u_{CDC})$. Resistances between phases are $R_{AC} = (R_A + R_C)$ and $R_{BC} = (R_B + R_C)$.

Hence, for the injected vectors v_1, v_3, and v_5, the per-phase equivalent resistances of the IM are obtained by solving (13)–(15), yielding

$$\mathbf{R}_{ABC} = \begin{bmatrix} 1 & 1 & 0 \\ 1 & 0 & 1 \\ 0 & 1 & 1 \end{bmatrix}^{-1} \begin{bmatrix} R_{AB} \\ R_{AC} \\ R_{BC} \end{bmatrix}. \tag{16}$$

Thereby, the following signal is proposed as an HRC indicator:

$$\mathbf{R}_{\mathrm{HRC}} = \mathbf{P}\, \mathbf{R}_{ABC} \tag{17}$$

where matrix $\mathbf{P}$ is defined as

$$\mathbf{P} = \begin{bmatrix} 1 & -\frac{1}{2} & -\frac{1}{2} \\ 0 & \frac{\sqrt{3}}{2} & -\frac{\sqrt{3}}{2} \end{bmatrix}. \tag{18}$$

This transformation eliminates the symmetric component of the resistance and projects asymmetric components into orthogonal coordinates, hereafter called the $\mathbf{R}_{\mathrm{HRC}}$ plane. Consequently, a vector in this plane shows the magnitude and direction of the resistance deviation from the symmetric condition.

If the IM is symmetrical, the value of $\mathbf{R}_{\mathrm{HRC}}$ is the null vector. As an example, if a symmetrical IM, whose stator resistance values are R_s, and an HRC problem (ΔR) in phase A are considered, the following expressions are obtained:

$$R_A = R_s + \Delta R \tag{19}$$

$$R_B = R_C = R_s. \tag{20}$$

In this case, the HRC indicator results

$$\mathbf{R}_{\mathrm{HRC}}|_{\mathrm{example}} = \begin{bmatrix} \Delta R \\ 0 \end{bmatrix}. \tag{21}$$

The previous example shows the low sensitivity of the HRC indicator to symmetrical variations of stator resistance, which can be produced by temperature increment.

It is worth noting that, although the IM equivalent circuit is presented in star connection in Fig. 5, the previous analysis is also valid for delta connection. This can be ensured due to the fact that the access to the neutral point of the IM is not necessary for the proposed method.

In addition, it is possible to highlight another important feature of this indicator, which is its low sensitivity to inductance variations produced by other IM asymmetries (e.g., stator winding turn faults, stator anisotropy, or air-gap eccentricity) due to the fact that it is calculated from the dc values of current and voltage signals.

The proposed HRC indicator does not need to be continuously computed due to the slow dynamic of the degradation mechanism of HRC [11], [12]. This feature makes it possible to apply the proposed signal injection method in certain time lengths during the normal operation of the IM. In this way, the effects of the improved dc signal injection over the IM performance are minimized. An analysis of these effects is presented in Section III-B.2.

As a final comment, it is important to note that the offset of the current sensors would introduce an error in the computed HRC indicator in a similar way as in [12]. To compensate it, the following procedure can be used: Before starting a sequence for determining the HRC indicator, the dc component of the phase currents is measured, whereas the injected dc signal is zero ($\mathbf{i}_{\alpha\beta\mathrm{dc}} = \mathbf{0}$). The dcs obtained in this way are the offsets and are subtracted from the measured currents when injecting the

TABLE II
IM RATED VARIABLES AND PARAMETERS

3 phase IM SIEMENS IE3 Model: 1LE1003-1CB09-0AB4-Z		
Variable/Parameter	**Value**	**Unit**
Power (P_n)	5.5	kW
Line Voltage (V_n)	400	V
Current (I_n)	10.5	A
Frequency (f_n)	50	Hz
Torque (T_e)	35	Nm
Efficiency (η)	89.6	%
Poles (P)	4	-
R_A	802.5	
R_B	811.5	mΩ
R_C	796.5	
R_s =mean($[R_A, R_B, R_C]$)	803.5	mΩ

vectors of Table I. This simple procedure was used to overcome the offset problems during the experimental validation of the HRC diagnosis method proposed in this effort.

III. EXPERIMENTAL VALIDATION OF PROPOSED METHOD

Here, the experimental setup used to validate the strategies of Section II and the experimental results are presented.

A. Experimental Setup

The proposed method for HRC diagnosis was implemented in a prototype, based on the block diagram of Fig. 2. The field-oriented control and the proposed method were implemented with an ×86-based PC, running the real-time operating system Linux-RTAI. A self-developed PCI interface implements the standard space-vector PWM and analog-to-digital conversions. The sampling frequency of the control algorithm is 10 kHz, and the switching frequency of the inverter is 5 kHz.

Although the strategy was programmed on a PC, it has a low computational requirement. For this reason, it can be easily implemented in a fixed-point microcontroller of a standard variable speed drive.

The diagnosis method was tested in a standard 5.5-kW IM, whose rated variables and parameters are provided in Table II. All results were obtained with IM stator windings connected in delta configuration.

As it was mentioned in [11], the most common HRC problems occur only in one phase of the incoming circuits of the IM. Therefore, the HRC was emulated with a resistance (ΔR) connected in series with IM phase A as in [11], [21], [23], [30]. Four different values of ΔR were used during the tests, namely 81.00, 170.70, 337.40, and 674.63 mΩ, which represent the 10.08%, 21.24%, 41.99%, and 83.96% of the mean value of stator resistances, respectively.

To evaluate the HRC indicator (17), two phase currents were measured and logged with the same PC used for the control. Details about current sensors are shown in Table III.

With the objective of validating the proposed diagnosis method with the IM under load, a second standard 5.5-kW IM with torque control was used as a load machine.

With the experimental setup described earlier, the results shown in the following were obtained.

TABLE III
CURRENT AND VOLTAGE SENSORS INFORMATION

Current sensors		
LEM LAH 25-NP		
Variable/Parameter	**Value**	**Unit**
Primary nominal current rms (I_{pn})	25	A
Accuracy	±0.3	%
Frequency Bandwidth(-1dB) (BW)	200	kHz
Voltage sensor (only used for comparison)		
Hameg Differential Probe HZ100		
Diff. input voltage (DC + peak AC) max.	±700	V
Accuracy	±3	%
Frequency Bandwidth(-1dB) (BW)	30/40	MHz

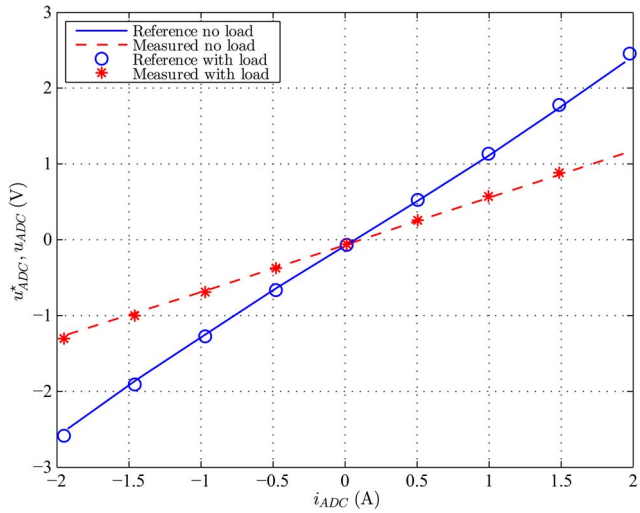

Fig. 6. Experimental results for reference and measured dc phase voltage versus dc phase current.

B. Experimental Results

1) Evaluation of the Inverter Nonlinearities Effects: As it was mentioned in Section II-B, inverter nonlinearities effects depend on the phase current direction ($i_{\text{phase}} < 0$ or $i_{\text{phase}} > 0$) because it determines the active switching devices (transistors or diodes) of the inverter during the operation.

Fig. 6 shows the dc phase A voltage behavior, reference and measured values, as function of the injected dc phase A current for the IM with and without load. The dc voltage was measured at the terminals of the IM with a differential voltage probe, through an analog low-pass filter whose cutoff frequency was set at 5 Hz. Details about the used voltage sensor are shown in Table III. The reference and measured values of the dc voltage are not affected by the load level of the IM, as it is shown in the figure. The value of the reference dc voltage for the IM with and without load are represented by a continuous line and circles, respectively, whereas by a dashed line and asterisks, respectively, for measured dc voltage.

Inverter nonlinearities produce a drop of the actual voltage with respect to the reference one (see Fig. 6). A linear relation (ohmic effect) between both dc voltages and currents is clearly observed, as it was analytically demonstrated by (12).

Based on these results, the voltage sensorless strategy and the inverter nonlinearities effects over the HRC indicator can be analyzed.

If (13) is expressed as function of reference phase voltages during the injection of v_1, the following expression is obtained:

$$R_{AB} = \frac{\left(u_{ADC}^{*v_1} - \overline{\Delta u}_A^{v_1}\right) - \left(u_{BDC}^{*v_1} - \overline{\Delta u}_B^{v_1}\right)}{i_{ADC}^{v_1}} \quad (22)$$

where $\overline{\Delta u}_A$ and $\overline{\Delta u}_B$ are the inverter dc voltage drops on phases A and B, namely, $\overline{\Delta u}_x = u_{x\mathrm{dc}} - u_{x\mathrm{dc}}^*$.

Considering that $i_{ADC}^{v_1} - i_{BDC}^{v_1} = 0$ and assuming $\overline{\Delta u}_A^{v_1} = -\overline{\Delta u}_B^{v_1} = \overline{\Delta u}$, the following expression is obtained:

$$R_{AB} = \frac{\left(u_{ADC}^{*v_1} - u_{BDC}^{*v_1}\right)}{i_{ADC}^{v_1}} - \frac{2\overline{\Delta u}}{i_{ADC}^{v_1}}. \quad (23)$$

For vectors 3 and 5, the same previous assumption can be done (namely, $\overline{\Delta u}_A^{v_3} = -\overline{\Delta u}_C^{v_3} = \overline{\Delta u}$ and $\overline{\Delta u}_B^{v_5} = -\overline{\Delta u}_C^{v_5} = \overline{\Delta u}$) due to $i_{ADC}^{v_3} = i_{BDC}^{v_5} = i_{ADC}^{v_1}$, yielding

$$R_{AC} = \frac{\left(u_{ADC}^{*v_3} - u_{CDC}^{*v_3}\right)}{i_{ADC}^{v_3}} - \frac{2\overline{\Delta u}}{i_{ADC}^{v_3}} \quad (24)$$

$$R_{BC} = \frac{\left(u_{BDC}^{*v_5} - u_{CDC}^{*v_5}\right)}{i_{BDC}^{v_5}} - \frac{2\overline{\Delta u}}{i_{BDC}^{v_5}}. \quad (25)$$

From (23)–(25), two important conclusions can be drawn.

- Inverter nonlinearities behave as a symmetrical variation of the equivalent resistance (second term of previous equations). This effect is similar to that produced by a temperature increment. This kind of effect was treated in the example of Section II-C, in which the low sensitivity of the HRC indicator to symmetrical variations was demonstrated. Therefore, it is possible to assert that the proposed strategy is not affected by inverter nonlinearities effects.
- The use of reference voltages to calculate the resistances is clearly observed in previous equations. This fact gives the proposed strategy in Section II the voltage sensorless characteristic, which implies an important reduction in the implementation costs and an increment in the robustness. The results shown in the following are obtained using this voltage sensorless strategy.

2) Perturbation of the Signal Injection: The effect of the injected signal on the torque of the machine, which was described in Section II-A, is evaluated experimentally here. Two tests have been performed with the IM turning at $\omega_m = 1200$ r/min without load. The direct dc signal injection as in (1) and (2) was used for the first test, yielding the variables shown in Fig. 7. In the upper plot, it can be observed that the currents in $\alpha\beta$ have a dominant sinusoidal component due to the magnetizing current. The α-component has an additional small dc component due to the direct injected signal. These currents transformed to the dq frame are shown in the middle plot. In normal steady-state operation without injected signal, they would be constant. With the injected signal, however, they have an oscillating component, as it can be observed in the figure. The oscillation of the q-component produces torque oscillation. The estimated rotor flux, which results from the d current, is almost constant due to the slow rotor time constant. This is shown in the middle plot and again in detail in the bottom one.

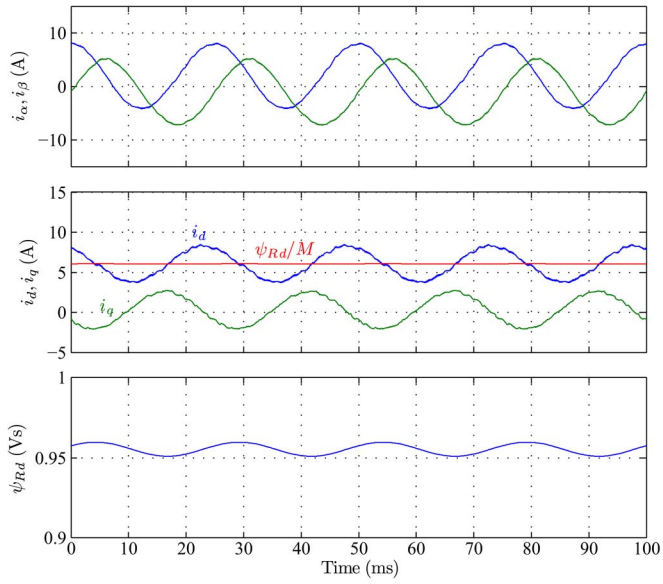

Fig. 7. Experimental results for direct dc signal injection. (a) Current in the $\alpha\beta$ reference frame. (b) Currents in the dq reference frame. (c) Rotor flux.

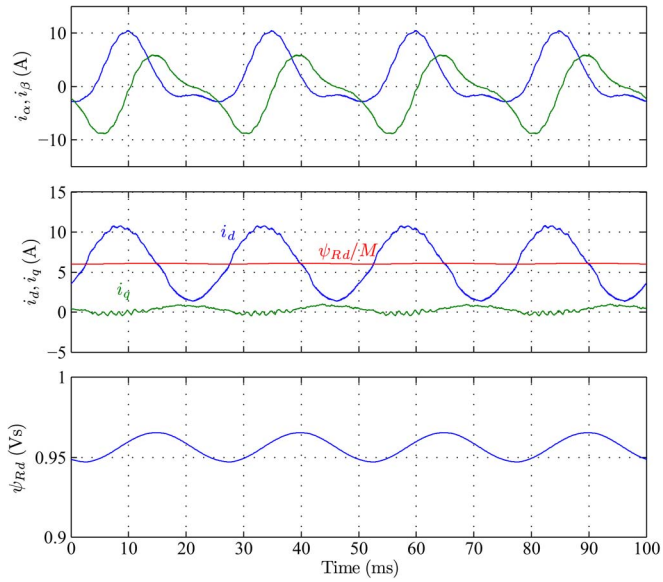

Fig. 8. Experimental results for improved dc signal injection. (a) Current in the $\alpha\beta$ reference frame. (b) Currents in the dq reference frame. (c) Rotor flux.

The proposed improved dc signal injection, as in (3) and (4), was used for the second test, whose results are shown in Fig. 8. The $\alpha\beta$ currents shown in the upper plot seem highly distorted; however, the α-current has the required dc component, being the respective q-component almost constant. The currents in the dq reference frame are shown in the middle plot. Although the d current has a higher oscillating component than in the case of direct dc signal injection, the rotor flux is still almost constant as shown in the middle and bottom plots.

The most important advantage of the improved dc signal injection is that the oscillation in the q-current and, consequently, in the torque is almost eliminated. This is clearly shown in Fig. 9, in which the speed for both tests are depicted. The

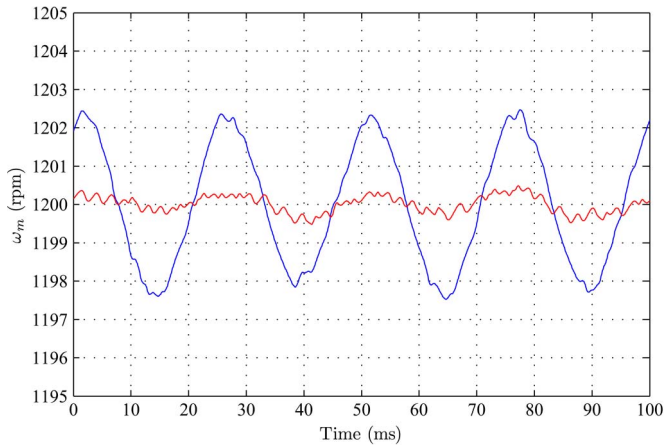

Fig. 9. Experimental results for speed at no load comparing the direct (blue) and improved (red) dc signal injection.

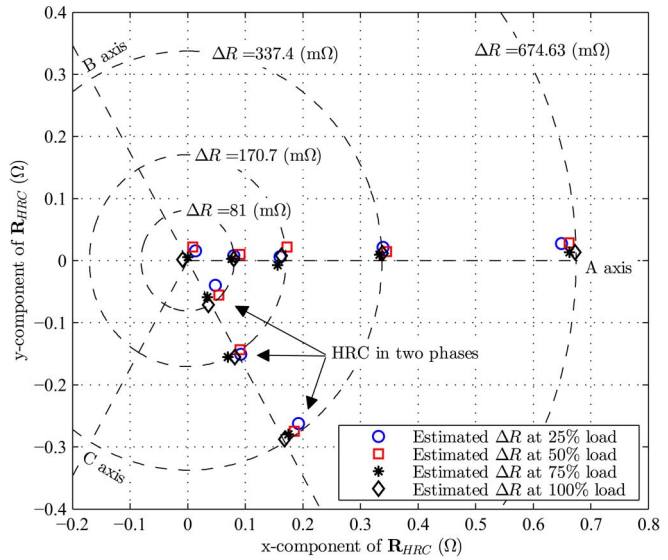

Fig. 10. Experimental results for the variation of $\mathbf{R}_{\mathrm{HRC}}$ with respect to contact resistance in one and two phases of the IM.

direct dc signal injection produces a speed oscillation of about ±2.5 r/min, whereas for the improved dc signal injection, it is only about ±0.5 r/min.

3) Evaluation of High-Resistance Connection: The experimental results shown here were obtained with the IM working at constant rotor speed ($\omega_m = 1200$ r/min). In this condition, the six vectors (see Table I) were injected. To evaluate the HRC indicator (17), the IM stator dcs and reference dc voltages were logged and processed on the PC.

Fig. 10 shows the $\mathbf{R}_{\mathrm{HRC}}$ plane in which the values of $\mathbf{R}_{\mathrm{HRC}}$ for different ΔR are drawn. The results shown in this figure were obtained with four different IM load levels, 25%, 50%, 75%, and 100% of the rated torque. To indicate the different values of ΔR, concentric circumferences were drawn.

As it was mentioned earlier, HRC were emulated in phase A. This becomes evident in Fig. 10 as the different points of $\mathbf{R}_{\mathrm{HRC}}$ appear in a small neighborhood of this axis. Furthermore, a small dispersion in the results as a consequence of the load variation is shown. This dispersion is due to the nonlinearities of the inverter and the current sensors and uncertainties in the

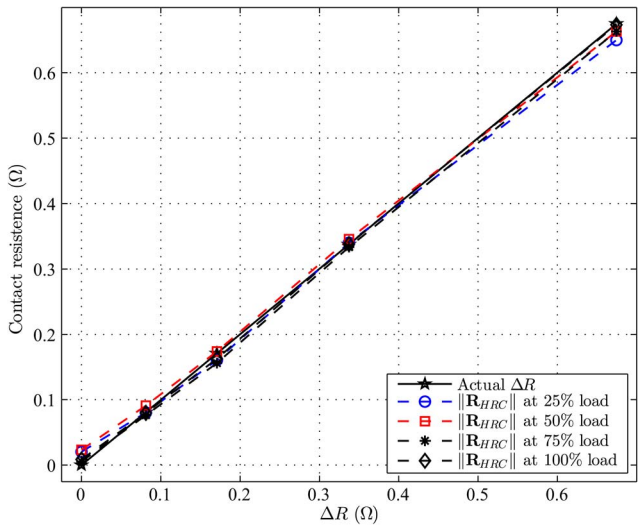

Fig. 11. Experimental results for the Euclidean norm of $\mathbf{R}_{\mathrm{HRC}}$ with respect to contact resistance for HRC in one phase.

measurement process. Despite this dispersion, the estimation of the contact resistance is not significantly affected. An analysis of the estimation error is presented in the following. Therefore, it is possible to assert that the proposed method is able to identify the faulty phase allowing then a rapid and precise troubleshooting.

In addition, in Fig. 10, certain inherent asymmetries in the winding phases for $\Delta R = 0$ are possible to note. Despite this fact, results show very good sensitivity to the variations of ΔR, even for its smallest value.

Fig. 11 compares the Euclidean norm of $\mathbf{R}_{\mathrm{HRC}}$ with the actual values of the emulated contact resistances ΔR for the aforementioned IM load conditions. The proposed method provides a good estimation of the contact resistance. The small differences between the actual and the estimated value of contact resistance can be quantified by the percentage relative error calculated as

$$e_r = \left(\frac{\Delta R - \|\mathbf{R}_{\mathrm{HRC}}\|}{R_s} \right) * 100\%. \tag{26}$$

The maximum error obtained for the resistance estimation was $e_{\mathrm{r-max}} = 3.06\%$, whereas the average error was $e_{\mathrm{r-avg}} = 1.09\%$ for the different load levels. We consider that these error values are low for the proposed method, showing its high accuracy in the estimation of HRC problems. Therefore, it is possible to assert that previous results demonstrate the validity of the proposed method to diagnose problems of HRC.

As it was mentioned in [11], the most common HRC problems occur in only one phase of the incoming circuits of the IM. Therefore, HRC was emulated with a resistance connected in series with IM phase A, as in [11] and [30].

Despite this fact, in this paper, HRC is considered in two phases of the IM to evaluate the validity of the proposed method. In this case, two resistances with the same value were connected to the phases A and C, repeating the test for 81, 170.7, and 337.4 mΩ.

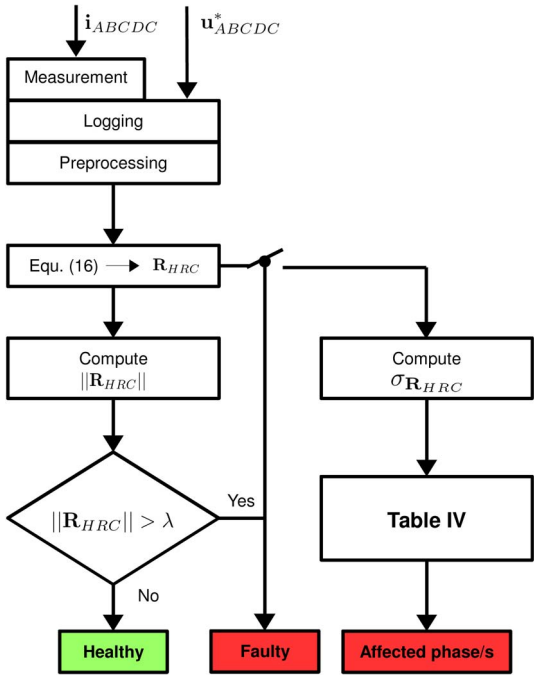

Fig. 12. Flowchart of FDI algorithm for the HRC problems.

Fig. 10 also shows the results obtained with the proposed method for HRC in two phases. These results were obtained with the same load levels aforementioned. By analyzing Fig. 10, it is noticed that experimental results, obtained with HRC in two phases, are placed in a small neighborhood around the bisector line between axis A and C (exactly $\pi/6$). This can be easily explained by taking into account that the geometrical composition of two vectors with the same Euclidean norm is always on the bisector line.

In a general case, in which ΔR_A and ΔR_C are marked differently, the proposed method will place points in a sector of the $\mathbf{R}_{\mathrm{HRC}}$ plane limited by axis A and C. The exact point will be given by the Euclidean norm and the angle of $\mathbf{R}_{\mathrm{HRC}}$, which can be calculated as

$$\sigma_{\mathbf{R}_{\mathrm{HRC}}} = \mathrm{atan2}\left(\mathbf{R}_{\mathrm{HRC}}(\mathrm{x}-\mathrm{comp}), \mathbf{R}_{\mathrm{HRC}}(\mathrm{y}-\mathrm{comp})\right). \tag{27}$$

The angle $\sigma_{\mathbf{R}_{\mathrm{HRC}}}$ makes it possible to identify the faulty phases as well as a rapid and precise troubleshooting for HRC problems in two phases.

Finally, it is important to remark the good correlation between actual and estimated values of contact resistance with different load levels, as in the case of HRC in one phase, validating in this way the proposed method for the case of HRC in two phases.

IV. Proposed Fault Detection and Isolation Algorithm

Here, an FDI algorithm for the diagnosis of HRC is proposed. Fig. 12 shows the flowchart schematizing the proposed FDI algorithm. The first step for the detection of HRC consists in the logging of reference dc phase voltages $(\mathbf{u}^*_{ABC\mathrm{DC}})$ and dc measured currents $(\mathbf{i}_{ABC\mathrm{DC}})$ for the different injected dc vectors. In addition, this step also involves the preprocessing of those signals to obtain dc line voltages, followed by the equivalent phase resistances (16).

In a second step, the proposed signal indicator (17) is computed.

Once (17) is calculated, the Euclidean norm $(\|\mathbf{R}_{\mathrm{HRC}}\|)$ is taken and compared with the limit $\boldsymbol{\lambda}$ for detecting and quantifying the HRC. If $\|\bullet\| > \boldsymbol{\lambda}$, the algorithm will return the faulty condition else the healthy one.

Furthermore, after the faulty condition is returned, the angle $\sigma_{\mathbf{R}_{\mathrm{HRC}}}$ is enabled to be computed by using (27). Based on this information, the faulty phases in which HRC appears are determined.

The following show how to determine the limits $\boldsymbol{\lambda}$ and the phases affected by HRC.

TABLE IV
Affected Phases Depending on Angle $\sigma_{\mathbf{R}_{\mathrm{HRC}}}$

Case	Angle limits	Affected phase/s
I	$0 < \sigma_{\mathbf{R}_{HRC}} < 2\pi/3$	a and b
II	$2\pi/3 < \sigma_{\mathbf{R}_{HRC}} < 4\pi/3$	b and c
III	$4\pi/3 < \sigma_{\mathbf{R}_{HRC}} < 2\pi$	c and a
IV	$\sigma_{\mathbf{R}_{HRC}} = 0$	a
V	$\sigma_{\mathbf{R}_{HRC}} = 2\pi/3$	b
VI	$\sigma_{\mathbf{R}_{HRC}} = 4\pi/3$	c

A. Determination of Limits for the HRC Alarms $(\boldsymbol{\lambda})$

Here, a description of the propose method to determine the limits for the HRC alarms $(\boldsymbol{\lambda})$ is presented.

By measuring the stator resistances of 15 new IMs, a maximum inherent asymmetry of 1.5% of the mean value between R_A, R_B, and R_C could be determined. These values can be taken as a reference for low power machines (all tested IM belong to this range of power < 10 kW).

In addition, the method error must be also taken into account for determining the limits for the HRC alarms. The maximum error was computed in Section III-B3, with a value of $e_{\mathrm{r-max}} = 3.06\%$.

Therefore, by considering these two values, the following limit for $\|\mathbf{R}_{\mathrm{HRC}}\|$ is proposed:

$$\boldsymbol{\lambda} = 4.56 * \mathrm{mean}\left([R_A, R_B, R_C]\right)/100. \tag{28}$$

This limit is compared with $\|\mathbf{R}_{\mathrm{HRC}}\|$ to obtain a signal alarm.

B. Determination of Phases in Which HRC Occurs

To identify the phases in which HRC occurs, the angle $\sigma_{\mathbf{R}_{\mathrm{HRC}}}$ must be computed as it was defined by (27). This value will be included in one of the six possible cases shown in Table IV. The second column of Table IV presents the angle limits for each case.

Once the angle is computed, it is possible to determine the faulted phases. The third column of Table IV shows the phases that are affected by HRC in each case.

V. Conclusion and Final Remarks

A new online voltage sensorless HRC diagnosis method based on signal injection was proposed in this effort. The theoretical underpinning of the signal injection method and the used HRC indicator were presented. For computing the proposed indicator ($\mathbf{R}_{\mathrm{HRC}}$), voltage references and stator current information were only required. Therefore, the proposed method only needs the use of two current sensors that are generally available in standard IM drives for the speed or torque control.

The diagnosis method was experimentally validated using a laboratory prototype. The possibility of detecting HRCs while determining their severity was demonstrated. In addition, the physical location of the HRC in the incoming circuit of the IM was demonstrated even for HRC in two phases. The high sensitivity of the proposed method was shown by estimating contact resistances of 10% of the rated value of R_s. All results were obtained with a very low estimation error and high immunity to symmetric variations in the IM stator resistance and those effects associated to the inverter (e.g., dead times).

Furthermore, the effects produced by the direct and the improved dc signal injection over the normal operation of the IM drive were analyzed in this paper. The low perturbation produced by the proposed improved injection method on the IM speed and currents was experimentally demonstrated. Although the resulting speed and current perturbations are small for most of the applications, they can be minimized even more by running the method for a few seconds every day. This fact is due to the slow dynamic of the degradation mechanism of HRC.

This low cost automatic HRC diagnosis method can be programmed in the microcontroller of the standard drive since it does not need large computational requirements nor database information of the IM. Moreover, the diagnosis method can be implemented in motors with both star and delta connections.

References

[1] H. Henao *et al.*, "Trends in fault diagnosis for electrical machines: A review of diagnostic techniques," *IEEE Ind. Electron. Mag.*, vol. 8, no. 2, pp. 31–42, Jun. 2014.

[2] A. Bellini, F. Filippetti, C. Tassoni, and G.-A. Capolino, "Advances in diagnostic techniques for induction machines," *IEEE Trans. Ind. Electron.*, vol. 55, no. 12, pp. 4109–4126, Dec. 2008.

[3] H. Henao, C. Demian, and G.-A. Capolino, "A frequency-domain detection of stator winding faults in induction machines using an external flux sensor," *IEEE Trans. Ind. Appl.*, vol. 39, no. 5, pp. 1272–1279, Sep./Oct. 2003.

[4] G. Joksimovic, J. Riger, T. Wolbank, N. Peric, and M. Vasak, "Stator-current spectrum signature of healthy cage rotor induction machines," *IEEE Trans. Ind. Electron.*, vol. 60, no. 9, pp. 4025–4033, Sep. 2013.

[5] V. Climente-Alarcon, J. Antonino-Daviu, M. Riera-Guasp, and M. Vlcek, "Induction motor diagnosis by advanced notch fir filters and the wigner-ville distribution," *IEEE Trans. Ind. Electron.*, vol. 61, no. 8, pp. 4217–4227, Aug. 2014.

[6] A. Soualhi, H. Razik, G. Clerc, and D. D. Doan, "Prognosis of bearing failures using hidden Markov models and the adaptive neuro-fuzzy inference system," *IEEE Trans. Ind. Electron.*, vol. 61, no. 6, pp. 2864–2874, Jun. 2014.

[7] K. Lee, J. Hong, K. Lee, S.-B. Lee, and E. Wiedenbrug, "A stator core quality assessment technique for inverter-fed induction machines," *IEEE Trans. Ind. Appl.*, vol. 46, no. 1, pp. 213–221, Jan./Feb. 2010.

[8] D. Campos-Delgado, D. Espinoza-Trejo, and E. Palacios, "Fault-tolerant control in variable speed drives: A survey," *IET Elect. Power Appl.*, vol. 2, no. 2, pp. 121–134, Mar. 2008.

[9] N. Freire and A. Marques Cardoso, "A fault-tolerant direct controlled pmsg drive for wind energy conversion systems," *IEEE Trans. Ind. Electron.*, vol. 61, no. 2, pp. 821–834, Feb. 2014.

[10] A. Mohammadpour, S. Sadeghi, and L. Parsa, "A generalized fault-tolerant control strategy for five-phase pm motor drives considering star, pentagon, and pentacle connections of stator windings," *IEEE Trans. Ind. Electron.*, vol. 61, no. 1, pp. 63–75, Jan. 2014.

[11] J. Yun, J. Cho, S. B. Lee, and J.-Y. Yoo, "Online detection of high-resistance connections in the incoming electrical circuit for induction motors," *IEEE Trans. Ind. Appl.*, vol. 45, no. 2, pp. 694–702, Mar./Apr. 2009.

[12] P. M. de la Barrera, G. R. Bossio, and J. A. Solsona, "High-resistance connection detection in induction motor drives using signal injection," *IEEE Trans. Ind. Electron.*, vol. 61, no. 7, pp. 3563–3573, Jul. 2014.

[13] P. M. de la Barrera, R. Leidhold, and G. R. Bossio, "On-line diagnosis of high-resistance connection for inverter fed induction motors," in *Proc. 7th IET Int. Conf. PEMD*, Manchester, U.K., 2014, pp. 1–5.

[14] V. Babrauskas, "How do electrical wiring faults lead to structure ignitions?" in *Proc. Fire Mater. Conf.*, London, U.K., 2001, pp. 39–51.

[15] F. Briz, M. Degner, J. Guerrero, and P. Garcia, "Stator windings fault diagnostics of induction machines operated from inverters and soft-starters using high-frequency negative-sequence currents," *IEEE Trans. Ind. Appl.*, vol. 45, no. 5, pp. 1637–1646, Sep./Oct. 2009.

[16] M. Braunovic, N. Myshkin, and V. Konchits, *Electrical Contacts: Fundamentals, Applications and Technology*. New York, NY, USA: Taylor & Francis, 2006.

[17] M. Baranski and A. Polak, "Thermal diagnostic in electrical machines," *Przeglad Elektrotech. (Elect. Rev.)*, no. 10, pp. 305–308, Oct. 2011.

[18] G. Stojcic, M. Vogelsberger, and T. Wolbank, "Detecting incipient stator winding conductor faults in inverter fed machines," in *Proc. 15th EPE Conf. Appl.*, Lille, France, 2013, pp. 1–9.

[19] G. Stojcic and T. M. Wolbank, "Detection of defects in stator winding of inverter fed induction machines," in *Proc. IEEE IEMDC*, Chicago, IL, USA, 2013, pp. 111–116.

[20] G. Stojcic and T. Wolbank, "Detecting high-resistance connection asymmetries in inverter fed AC drive systems," in *Proc. 9th IEEE Int. SDEMPED*, Valencia, Spain, 2013, pp. 227–232.

[21] Y. Gritli *et al.*, "Advanced diagnosis of electrical faults in wound-rotor induction machines," *IEEE Trans. Ind. Electron.*, vol. 60, no. 9, pp. 4012–4024, Sep. 2013.

[22] Y. Gritli, L. Zarri, C. Rossi, F. Filippetti, and D. Casadei, "Fault detection and quantification of stator high-resistance connection for induction machines," in *Proc. IEEE ICSD*, Bologna, Italy, 2013, pp. 113–116.

[23] L. Zarri *et al.*, "Detection and localization of stator resistance dissymmetry based on multiple reference frame controllers in multiphase induction motor drives," *IEEE Trans. Ind. Electron.*, vol. 60, no. 8, pp. 3506–3518, Aug. 2013.

[24] L. Zarri *et al.*, "Full detection of high-resistance connections in multiphase induction machines," in *Proc. 9th IEEE Int. SDEMPED*, Valencia, Spain, 2013, pp. 505–511.

[25] L. Zarri *et al.*, "On-line detection of high resistance connections with inverse-sequence regulators in three phase induction motor drives," in *Proc. IEEE ECCE*, Denver, CO, USA, 2013, pp. 4426–4431.

[26] L. Zarri *et al.*, "On-line detection of high resistance connections with negative-sequence regulators in three phase induction motor drives," in *Proc. IEEE ECCE*, Denver, CO, USA, 2013, pp. 4426–4431.

[27] S. Cheng, Y. Du, J. A. Restrepo, P. Zhang, and T. G. Habetler, "A nonintrusive thermal monitoring method for induction motors fed by closed-loop inverter drives," *IEEE Trans. Power Electron.*, vol. 27, no. 9, pp. 4122–4131, Sep. 2012.

[28] N. Urasaki, T. Senjyu, K. Uezato, and T. Funabashi, "Adaptive dead-time compensation strategy for permanent magnet synchronous motor drive," *IEEE Trans. Energy Convers.*, vol. 22, no. 2, pp. 271–280, Jun. 2007.

[29] K. Wiedmann, F. Wallrapp, and A. Mertens, "Analysis of inverter nonlinearity effects on sensorless control for permanent magnet machine drives based on high-frequency signal injection," in *Proc. 13th EPE Conf. Appl.*, Barcelona, Spain, 2009, pp. 1–10.

[30] D. Patel and M. Chandorkar, "On-line load test for induction machine stator inter-turn fault detection under stator electrical asymmetries," in *Proc. 36th IEEE IECON*, Glendale, AZ, USA, 2010, pp. 933–938.

Pablo M. de la Barrera (S'99–S'08–M'09) was born in Río Cuarto, Argentina, in 1978. He received the B.Sc. and M.Sc. degrees in electrical engineering from the Universidad Nacional de Río Cuarto, Río Cuarto, in 2003 and 2006, respectively, and the Ph.D. degree in control systems from the Universidad Nacional del Sur, Bahía Blanca, Argentina, in 2009.

Since 1998, he has been with the Grupo de Electrónica Aplicada, Universidad Nacional de Río Cuarto. He is also currently with the Consejo Nacional de Investigaciones Científicas y Técnicas (CONICET), Buenos Aires, Argentina.

Dr. de la Barrera is currently the Secretary of the Argentina Section Joint Chapter within the IEEE (IE13/CS23/RA24/IA34/PEL35/VT06).

Guillermo R. Bossio (S'03–M'07) received the B.Sc. degree in electrical engineering from the Universidad Nacional de Río Cuarto, Río Cuarto, Argentina, in 1999 and the Ph.D. degree in engineering from the Universidad Nacional de La Plata, La Plata, Argentina, in 2004.

Since 1994, he has been with Grupo de Electrónica Aplicada, Facultad de Ingeniería, Universidad Nacional de Río Cuarto. He is also currently with the Consejo Nacional de Investigaciones Científicas y Técnicas, Buenos Aires, Argentina. His research interests include fault diagnosis of electric machines, ac motor drives, electric vehicles, and renewable energy generation.

Roberto Leidhold (S'94–M'03) received the B.S. degree in electronics engineering from the Universidad Nacional de Córdoba, Córdoba, Argentina, in 1995, the M.S. degree from the Universidad Nacional de Río Cuarto, Río Cuarto, Argentina, in 2000, and the Ph.D. degree from the Universidad Nacional de La Plata, La Plata, Argentina, in 2003.

From 2003 to 2004, he was a Postdoctoral Fellow with the Universidad Nacional de Río Cuarto. From 2005 to 2011, he was with the Technical University of Darmstadt, Darmstadt, Germany, first as a Research Scholar of the Alexander von Humboldt Foundation, then as a Research Associate, and later as a Principal Investigator. Since 2011, he has been a Professor of electric drive systems with the Otto-von-Guericke-Universitaet Magdeburg, Magdeburg, Germany. His research interests include control of drives, electric machines, and renewable energy generation.